ACS APPLIED MATERIALS & INTERFACES

Research Article

www.acsami.org

Influence of Carbon Alloying on the Thermal Stability and Resistive Switching Behavior of Copper-Telluride Based CBRAM Cells

Wouter Devulder,*[,†] Karl Opsomer,[‡] Felix Seidel,[‡,§] Attilio Belmonte,[‡,§] Robert Muller,[‡] Bob De Schutter,[†] Hugo Bender,[‡] Wilfried Vandervorst,[‡,§] Sven Van Elshocht,[‡] Malgorzata Jurczak,[‡] Ludovic Goux,[‡] and Christophe Detavernier[†]

[†]Department of Solid State Sciences, Universiteit Gent, Krijgslaan 281 (S1), 9000 Gent, Belgium

[‡]IMEC, Kapeldreef 75, 3001 Leuven, Belgium

[§]Department of Physics and Astronomy, KU Leuven, Celestijnenlaan 200D, 3001 Leuven, Belgium

Supporting Information

ABSTRACT: We report the improved thermal stability of carbon alloyed $Cu_{0.6}Te_{0.4}$ for resistive memory applications. Copper−tellurium-based memory cells show enhanced switching behavior, but the complex sequence of phase transformations upon annealing is disadvantageous for integration in a device. We show that addition of about 40 at % carbon to the Cu-telluride layer results in an amorphous material up to 360 °C. This material was then integrated in a TiN/$Cu_{0.6}Te_{0.4}$-C/Al_2O_3/Si resistive memory cell, and compared to pure $Cu_{0.6}Te_{0.4}$. Very attractive endurance (up to 1×10^3 cycles) and retention properties (up to 1×10^4 s at 85 °C) are observed. The enhanced thermal stability and good switching behavior make this material a promising candidate for integration in memory devices.

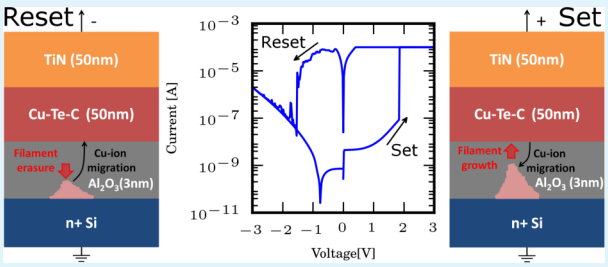

KEYWORDS: *resistive memory, CBRAM, ECM, Cu−Te, thermal stability, carbon alloying*

INTRODUCTION

The increasing demand for smaller, faster, and less-power-consuming memories has driven research for new types of memories. Among the emerging technologies, resistive random access memory (RRAM) seems very promising, combining low power and fast operation with good scalability.[1] One type of RRAM is conductive bridge RAM (CBRAM). Such a memory cell consists of a Cu or Ag containing electrode which acts as a cation source, an insulating layer that serves as electrolyte for metal cation drift, and an inert electrode. Applying a positive electrical potential on the active electrode induces cation drift through the insulating layer.[1,2] A conductive filament is grown and the cell switches to a low resistive state (LRS) when the filament bridges the two electrodes. By applying a negative potential, the cations drift back to the supply layer and the cell returns to a high resistive state (HRS). For the electrolyte layer, chalcogenide materials like Ag_2S,[3] Cu_2S,[4] GeSe,[5,6] and GeS[7] and organic materials[8] have been used. Recently, binary metal oxides like HfO_2,[9] Ta_2O_5,[2] ZrO_2,[10] SiO_2[11,12] and Al_2O_3[13] were introduced and are very promising because of their high compatibility with the fabrication of complementary metal oxide semiconductor (CMOS) devices. Next to pure Cu or Ag as active electrode, alloys containing Cu have been reported.[14,15] Very good memory properties have been demonstrated for the Cu−Te alloy,[15] moreover a strong influence of the Cu−Te composition on the switching properties of a Pt/Cu_xTe_{1-x}/Al_2O_3/Si memory cell was shown, with enhanced switching behavior in the range $0.5 < x < 0.7$[13] (henceforth referred to as $Cu_{0.6}Te_{0.4}$). However, the thermal stability of $Cu_{0.6}Te_{0.4}$ turns out to be limited, showing multiple phase transitions upon annealing.[16] For integration in a device, a material that is stable up to 400 °C is necessary. In this work, we use carbon as an alloying element to stabilize the $Cu_{0.6}Te_{0.4}$ source layer. Carbon is chosen because it does not form a carbide phase with Cu or Te, and hence will not introduce new phases next to the copper telluride phases. We show that the alloying element inhibits the phase formation up to 360 °C, creating a large thermal window where no transformation of the material occurs. The material is then used as a Cu-supply layer in a CBRAM cell, showing good switching behavior as deposited and after annealing for 5 min at 200 °C. The improved thermal stability and good switching behavior make this material a promising candidate for integration in memory devices.

EXPERIMENTAL SECTION

The mixed Cu−Te−C layer is deposited by DC-magnetron sputtering, using a commercial Balzers BAS 450 deposition tool. Materials properties were investigated on n-doped Si(100) substrates, covered with a 20 nm thin Al_2O_3 layer, deposited by an H_2O-based Atomic

Received: March 27, 2013
Accepted: July 4, 2013
Published: July 4, 2013

layer deposition (ALD) technique. The substrates are mounted on a rotating carousel in the deposition chamber with a base pressure of 5×10^{-7} mbar. The layer is then deposited by cosputtering from three different sputter targets. The substrates on the rotating carousel pass subsequently in front of each sputter target, resulting in a closely intermixed Cu−Te−C layer. The composition of the layer was determined by energy-dispersive X-ray spectroscopy (EDX), using a FEI Quanta 200F FEG scanning electron microscope (SEM) equipped with an Edax Genesis 4000 EDX detector. Additionally, X-ray fluorescence spectroscopy (XRF) was used to verify the Cu and Te content (carbon cannot be detected with XRF). The composition could be determined after calibrating both systems using a reference sample that was characterized by Rutherford backscattering spectroscopy (RBS) and elastic recoil detection (ERD) for the Cu/Te and Cu/C ratio, respectively. X-ray photoelectron spectroscopy (XPS) was used both for investigation of the chemical bonds between Cu, Te and C and for composition determination. These are carried out on an S-Probe monochromatized XPS spectrometer of Surface Science Instruments (VG), using monochromatic Al K_α radiation (1486.6 eV) under a base pressure of 1×10^{-9} mbar. The photoelectron emission direction and the plane of the sample is kept constant at 45°. Depth profiling and hence information about the bulk of the material was obtained by abrasion of the surface by Ar^+ sputtering. Charging of the sample was eliminated using an electron flood gun.

Table 1 summarizes the results of the composition determination using these techniques. A Cu/Te ratio of 1.5 was pursued, as this ratio

Table 1. Composition of the 50 nm Cu−Te−C Mixed Layer Determined by EDX, XPS, and XRF

	C (at %)	Cu (at %)	Te (at %)
EDX	36.3	39.3	24.4
XPS	34.1	42.5	23.4
XRF		60.96	39.04

showed enhanced switching behavior,[13] whereas the carbon content was aimed to be about 40 at %. A nearly perfect 1.5 ratio of copper and tellurium is obtained, and the carbon content is close to 40 at %. Henceforth this composition will be referred to as $Cu_{0.6}Te_{0.4}$-C.

The stability of the material against phase transformations is investigated by means of in situ X-ray Diffraction (XRD). A material which is stable and does not transform under annealing is favorable to survive the thermal budget it receives in the process flow of device manufacturing. In situ XRD allows us to characterize the phase formation as function of temperature and hence gives us information about the thermal stability. A home-built setup consisting of a heating chamber mounted in a Bruker D8 Discover XRD system is used. The samples are subjected to a constant heating rate of 0.5 °C/s under an inert He atmosphere while a diffraction pattern was recorded every 4 s over a fixed 2θ window.

To study the microstructure of the material, the samples are investigated by high-resolution transmission electron microscopy (HR-TEM), using a FEI Technai F30 ST microscope. The TEM specimen were prepared with a FEI Dual Beam FIB/SEM STRATA 400, using the in situ lift-out technique, and milled electron transparent with a 30 keV Ga^+ ion beam. A spin on carbon (SOC) and Pt layer were deposited prior to the lift-out, to protect the surface from Ga^+ beam damage.

Next to the material properties, the functionality of the stabilized $Cu_{0.6}Te_{0.4}$-C layer as a Cu-supply layer in CBRAM is investigated. The $Cu_{0.6}Te_{0.4}$-C is integrated in a 580 μm diameter CBRAM cell and the resistive switching behavior is compared to a memory cell with pure $Cu_{0.6}Te_{0.4}$. The cells are prepared by subsequently magnetron sputtering of 50 nm $Cu_{0.6}Te_{0.4}$(-C) and 50 nm TiN through a dot shadow mask on a Si substrate covered with 3 nm thin Al_2O_3. The memory cells are characterized using a Keithley 2601A sourcemeter, operating in linear voltage sweep mode, with a constant sweep rate of 0.33 V/s. The cells are switched to a LRS and HRS by applying a double linear voltage sweep from respectively 0 V to +3 V (and back) and 0 V to −3 V (and back). During the set operation, the current is limited to 100 μA (compliance current I_c) to protect the cell from breakdown.

RESULTS AND DISCUSSION

Thermal Stability. Figure 1a compares the XRD patterns of the pure and carbon alloyed as deposited $Cu_{0.6}Te_{0.4}$(-C) layer.

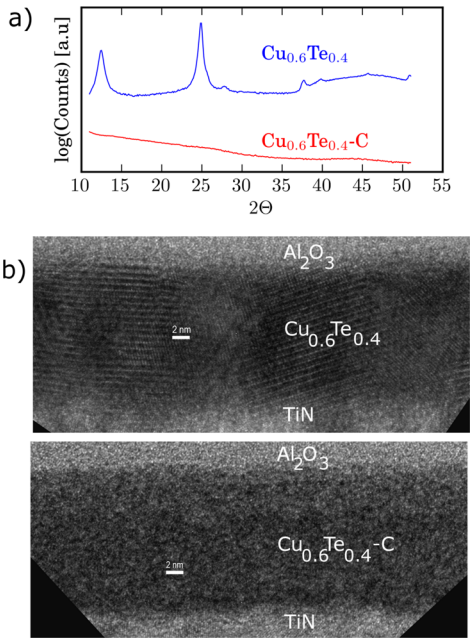

Figure 1. (a) XRD pattern of a $Cu_{0.6}Te_{0.4}/Al_2O_3$ and $Cu_{0.6}Te_{0.4}$-C/Al_2O_3 (50 nm/20 nm) sample. (b) HR-TEM image of a pure and a carbon alloyed TiN/$Cu_{0.6}Te_{0.4}$(-C)/Al_2O_3 (40/15/4 nm) sample, showing the $Cu_{0.6}Te_{0.4}$(-C) layer.

The (003) and (006) peaks of hexagonal $Cu_{2-x}Te$[17] at 12.28 and 24.72°, respectively, are clearly visible for pure $Cu_{0.6}Te_{0.4}$. In contrast, no diffraction peaks are observed for the $Cu_{0.6}Te_{0.4}$-C, suggesting it is in an amorphous state. The amorphous nature of the $Cu_{0.6}Te_{0.4}$-C is also confirmed by TEM. Figure 1b shows the HR-TEM images of both layers. Although for the pure $Cu_{0.6}Te_{0.4}$ the presence of Moiré fringes confirms the polycrystalline nature of the film, the C-alloyed layer instead evidently misses these Moiré fringes and therefore is amorphous or very small grained. HR-TEM reveals the presence of some small nanocrystals, which cannot be detected by XRD. From these results, it is clear that already during deposition the carbon atoms suppress the formation of a polycrystalline Cu−Te layer.

Figure 2 shows the XPS spectra of the C 1s, Cu $2p^{3/2}$, and Te $3d^{5/2}$ regions of both samples. The peaks for bulk C, Cu and Te, measured from a reference sample fabricated by magnetron sputtering of the pure elements on 100 nm SiO_2, are also shown. All spectra are calibrated to the C 1s transition at 284.6 eV of the hydrocarbon from contamination on the sample surface. The maximum of the carbon 1s peak of bulk carbon is situated at 284.4 eV, whereas the carbon peak for the $Cu_{0.6}Te_{0.4}$-C sample is slightly shifted over 0.25 eV toward lower energies. However, with a maximum at 284.15 eV, this is still in the reported range for C−C bonds.[18−20] This suggests that the carbon is mainly bonded with other carbon atoms. This was to be expected as no carbides are formed with Cu and Te. The pure Cu $2p^{3/2}$ and Te $3d^{5/2}$ peaks are located at

dx.doi.org/10.1021/am4010946 | ACS Appl. Mater. Interfaces 2013, 5, 6984−6989

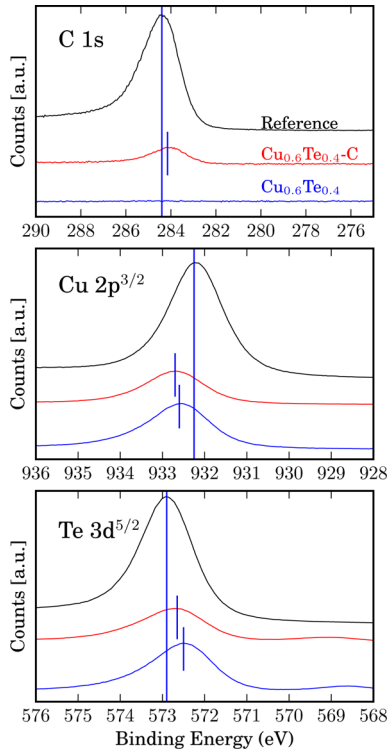

Figure 2. XPS measurement showing the C 1s, Cu $2p^{3/2}$ and Te $3d^{5/2}$ peaks. In each graph, the reference peak of pure C, Cu, or Te is given and the measured peak of both the $Cu_{0.6}Te_{0.4}$-C and $Cu_{0.6}Te_{0.4}$ sample.

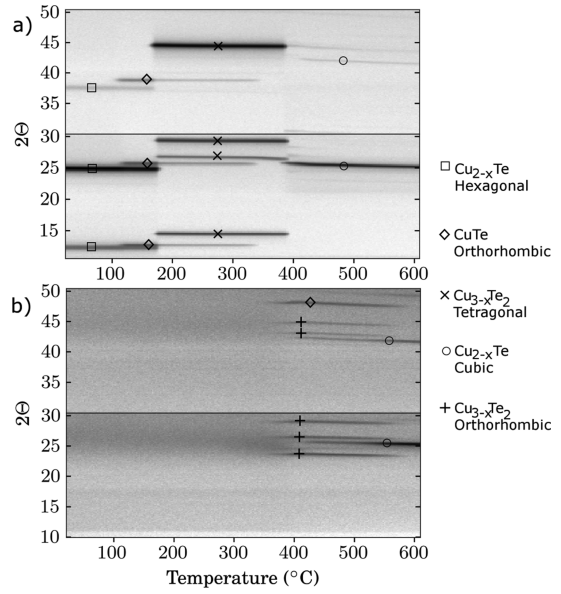

Figure 3. In situ XRD pattern, measured at a constant heating rate of 0.5 °C/s, of a $Cu_{0.6}Te_{0.4}$(-C)/Al_2O_3 (50 nm/20 nm) stack (a) without carbon and with (b) 40 at % carbon.

respectively 932.25 and 572.9 eV. For pure $Cu_{0.6}Te_{0.4}$, hexagonal $Cu_{2-x}Te$ is observed by XRD (see Figure 1a) and reveals the presence of Cu−Te bonds. In the XPS spectra, this is visible as a shift of the Cu $2p^{3/2}$ peak toward higher energy (932.6 eV, Cu is oxidized) and a shift of the Te $3d^{5/2}$ toward lower energy (572.5 eV, Te is reduced). The shifts are rather small, as reported in literature for tellurides.[21−23] For $Cu_{0.6}Te_{0.4}$-C, the peaks are also shifted with respect to the pure Cu and Te (932.7 eV for Cu $2p^{3/2}$ and 572.65 eV for Te $3d^{5/2}$), and small differences with $Cu_{0.6}Te_{0.4}$ are observed. It is very difficult to unambiguously analyze the difference between $Cu_{0.6}Te_{0.4}$-C and $Cu_{0.6}Te_{0.4}$, but the slightly shifted Cu peak might be related to a mix of Cu(I) and Cu(II) oxidation states in $Cu_{0.6}Te_{0.4}$-C, while merely Cu(I) is expected in $Cu_{0.6}Te_{0.4}$ due to the $Cu_{2-x}Te$ phase.[21] The small difference in binding energy for the Te peak might indicate the presence of more pure Te in $Cu_{0.6}Te_{0.4}$-C. However, the shifts indicate that also for $Cu_{0.6}Te_{0.4}$-C the copper is oxidized by the presence of Te, suggesting bonds between Cu and Te atoms.

Both samples are investigated with in situ XRD to study the phase stability upon annealing. Figure 3a shows the in situ XRD pattern of a $Cu_{0.6}Te_{0.4}/Al_2O_3/Si$ stack, exhibiting multiple phase transitions. As deposited, hexagonal $Cu_{2-x}Te$[17] is present. At 120 °C orthorhombic CuTe[24] is also formed. Both phases react and form tetragonal $Cu_{3-x}Te_2$[25] at 180 °C, but some CuTe is still present up to 350 °C. Finally, cubic $Cu_{2-x}Te$[26] is formed for T > 400 °C. These subsequent transformations are in agreement with the phase diagram.[27] The in situ XRD plot of the $Cu_{0.6}Te_{0.4}$-C layer (Figure 3b) clearly shows the absence of any diffraction peaks up to 360 °C, suggesting an amorphous layer up to this temperature, and hence a large temperature window where no transformation of the material occurs. The integrated XRD-intensity in the 11−31° 2θ window (see Figure S1 in the Supporting Information) starts to increase from 270 °C on, and reaches a local maximum at 360 °C, where distinct diffraction peaks appear. We define this temperature as the crystallization temperature of the $Cu_{0.6}Te_{0.4}$-C layer. The diffraction peaks are identified as orthorhombic $Cu_{3-x}Te_2$[28] and CuTe,[24] and cubic $Cu_{2-x}Te$.[26] The (111) and (010) peaks of graphite[29] coincide with the (052) and (154) peaks of $Cu_{3-x}Te_2$ at ∼26.6 and ∼43.5°, respectively. However, the disappearance of these peaks above 580 °C together with the other peaks of $Cu_{3-x}Te_2$ suggest no contribution of graphite. After crystallization of the Cu-telluride phases, the carbon is most likely at the grain boundaries of the copper−tellurium crystals. We believe that the inhibited phase formation is mainly related to kinetic aspects and the microstructure of the material. The combination of rather large elements like Cu and Te with a small element like C increases the packing density in the amorphous solid, which makes interdiffusion difficult. This impedes the rearrangement in a crystalline structure and hence inhibits the crystallization.[30] The increased thermal stability of amorphous alloys due to addition of small atoms like Be and C has been reported before,[31,32] showing an increased crystallization temperature after glass transition. Moreover, differential scanning calorimetry (DSC) of carbon doped $Zr_{41}Ti_{14}Cu_{12.5}Ni_9Be_{22.5}C_1$ showed a decrease in crystallization enthalpy, meaning that the formation of crystal phases becomes also thermodynamically less favorable compared to the undoped material.

Figure 4a shows the XRD pattern of both the pure and the C-alloyed $Cu_{0.6}Te_{0.4}$(-C)/Al_2O_3 stack after 5 min anneal at 300 °C, confirming the results of the in situ XRD measurements. The increased integrated intensity above 270 °C in the in situ XRD pattern and the somewhat broad maximum around 25° in Figure 4a suggest the presence of nanocrystals at higher temperatures. This is reasonable as with TEM nanocrystals could be observed even in the as deposited layer. A 50 nm TiN capping layer is further added to preserve a good surface morphology, and at the same time can serve as top electrode in a memory device. SEM analysis (Figure 4b) shows a very

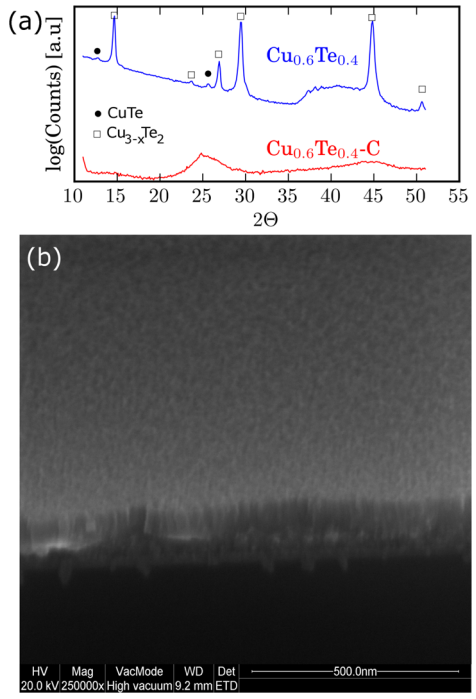

Figure 4. (a) XRD pattern of a pure and a C-alloyed $Cu_{0.6}Te_{0.4}$(-C)/Al_2O_3/Si stack after a 5 min anneal at 300 °C under He-atmosphere. (b) SEM image showing the surface morphology of the C-alloyed stack, capped with a 50 nm TiN layer after annealing for 5 min at 400 °C.

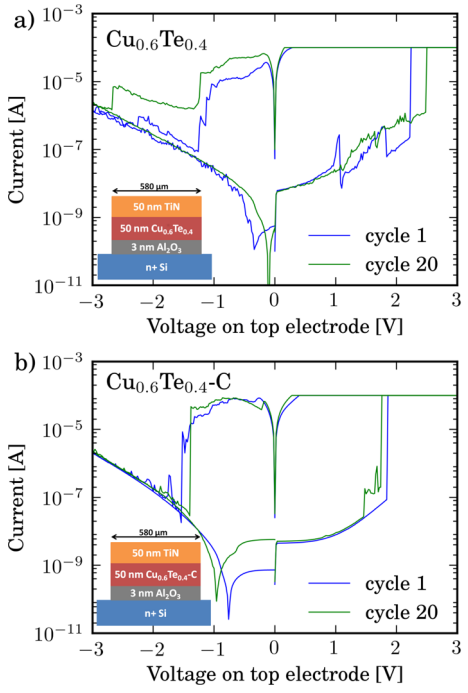

Figure 5. First and 20th set−reset operation of (a) pure and (b) C-alloyed TiN/$Cu_{0.6}Te_{0.4}$(-C)/Al_2O_3/Si memory cells.

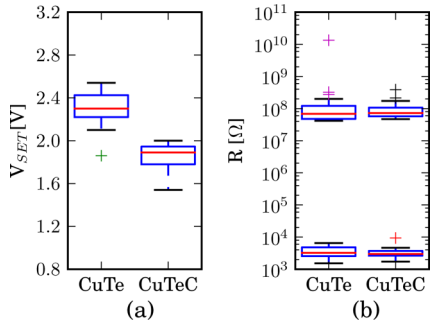

Figure 6. (a) Set voltage and (b) the resistance of the LRS and HRS of a pure and a C-alloyed TiN/$Cu_{0.6}Te_{0.4}$(-C)/Al_2O_3/Si memory cell. The data are presented in a boxplot, indicating the first, second (median) and third quartile. The whiskers extend form the box and are maximum 1.5 times the inner quartile length (if any data reaches this value). The crosses are flyer points, falling out of this region.

smooth surface morphology up to 400 °C. To conclude this section, the large temperature window without phase transformations combined with a good surface morphology up to 400 °C show the improved thermal stability of the TiN capped $Cu_{0.6}Te_{0.4}$-C layer compared to pure $Cu_{0.6}Te_{0.4}$, rendering his material attractive for integration in memory devices.

Integration in a CBRAM Device. The functionality of the stabilized $Cu_{0.6}Te_{0.4}$-C as Cu-supply layer in a CBRAM cell is investigated and compared to CBRAM cells with pure $Cu_{0.6}Te_{0.4}$. The 580 μm diameter dot CBRAM cells are cycled 20 times, from which the set voltage and the resistance of the LRS and HRS state is determined. Figure 5 shows the first and 20th set−reset cycle for both the pure and the C-alloyed $Cu_{0.6}Te_{0.4}$(-C) sample. The first cycle is the forming step, where Cu is driven into the Al_2O_3 layer to form a conductive filament (this in contrast to most chalcogenide systems were Cu or Ag is already present in the resistive switching layer). However, the set voltage of the first cycle and the subsequent cycles are the same, showing no difference between the forming and the subsequent cycles. This indicates an effective erasure of the entire filament after reset. This dependence of the set voltage on the partial or complete erasure of the filament has been pointed out before.[33] It is clear that the C-alloyed cell shows a good switching behavior and is very comparable to pure $Cu_{0.6}Te_{0.4}$. The reset current of both cells is comparable and lower than I_c, which leads to an efficient reset, as was already reported for pure $Cu_{0.6}Te_{0.4}$.[13] The set voltage (Figure 6a) of the C-alloyed cell is slightly lower than for pure $Cu_{0.6}Te_{0.4}$. Although the resistivity of the $Cu_{0.6}Te_{0.4}$-C is higher than $Cu_{0.6}Te_{0.4}$ (9.54×10^{-3} Ω cm and 2.99×10^{-4} Ω cm respectively), this is still many orders of magnitude lower than Al_2O_3.[34] As a result, the resistance of the layer will not affect the set voltage because the voltage will always drop over the Al_2O_3.

The lower set voltage may be attributed to the amorphous nature of the $Cu_{0.6}Te_{0.4}$-C layer. The amorphous state is a metastable state, and the Cu has a lower binding energy than in a crystal structure. From this point of view, a lower potential may already result in the removal of Cu ions from the source layer compared to a crystalline material. However, we do not want to exclude the presence of pure Cu, which has a lower set voltage because of the lower bonding energy of Cu compared to Cu−Te.[13] The pure Cu can be present in nanocrystals, which cannot be detected with XRD. Figure 6b shows a boxplot of the resistance of the LRS and HRS of both cells, which turn out to be very comparable.

To be a viable candidate as CBRAM source layer, good endurance and retention properties should be observed. The $Cu_{0.6}Te_{0.4}$-C memory cell was cycled up to 1000 times at room temperature, and after annealing for 5 min at 200 °C in He atmosphere (both with I_c = 100 μA). Figure 7a shows the cumulative distribution of the HRS and LRS for both the as

dx.doi.org/10.1021/am4010946 | ACS Appl. Mater. Interfaces 2013, 5, 6984−6989

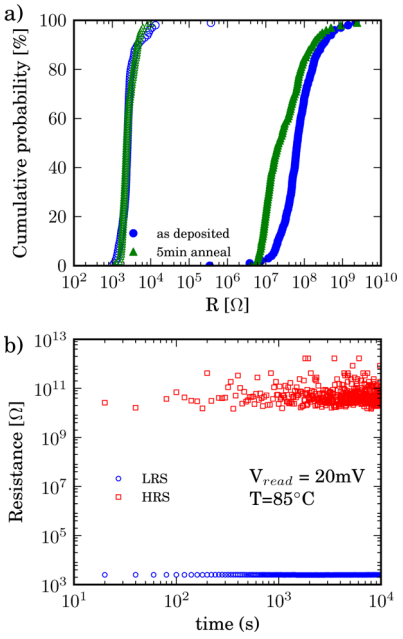

Figure 7. (a) Cumulative probability of the LRS (open markers) and HRS (filled markers) of the memory cell as deposited and after anneal (5 min at 200 °C). (b) Retention test at 85 °C and using a constant read bias of 20 mV. The LRS and HRS are not altered for up to 10^4 s.

deposited and annealed device (see Figure S2 in the Supporting Information for the detailed endurance results). Even after annealing, the difference between the LRS and HRS is more than 2 orders of magnitude, although a small shift of the HRS toward lower resistances is observed. This could be related to Cu diffusion into the Al_2O_3 layer. As a suggestion for future work, this might be further improved by adding a titanium diffusion barrier in between the $Cu_{0.6}Te_{0.4}$-C layer and the aluminum oxide.[16] The retention was tested by applying a constant read voltage of 20 mV at an elevated temperature of 85 °C. The LRS and HRS did not change for up to 1×10^4 s (Figure 7b), proving the stability of the states.

CONCLUSIONS

We showed the ability of carbon to influence the crystallization and stability of copper tellurium. Adding about 40 at % C to a Cu_xTe_{1-x} ($x \approx 0.6$) layer results in an amorphous material up to 360 °C. We attribute this inhibited phase formation to an increased packing density in the amorphous solid, making the rearrangement in a crystalline structure much more difficult. A TiN capping layer on top ensures a good surface morphology up to 400 °C and serves as a top electrode. A functional memory cell was demonstrated, showing controlled switching and good reliability characteristics.

ASSOCIATED CONTENT

Supporting Information

The integrated intensity over the 11−31° 2θ window of the in situ XRD pattern of the $Cu_{0.6}Te_{0.4}$-C layer as a function of the temperature. The detailed endurance results of the TiN/$Cu_{0.6}Te_{0.4}$-C/Al_2O_3/n + Si memory cells, as deposited and after 5 min anneal at 200 °C. This material is available free of charge via the Internet at http://pubs.acs.org/.

AUTHOR INFORMATION

Corresponding Author

*E-mail: Wouter.Devulder@UGent.be. Phone: +32 (0) 9 264 43 48. Fax: +32 (0) 9 264 49 96.

Notes

The authors declare no competing financial interest.

ACKNOWLEDGMENTS

W.D. acknowledges the Institute for the Promotion of Innovation through Science and Technology in Flanders (IWT-Vlaanderen) for funding. Nico De Roo and Johan Meersschaut are acknowledged for physical characterization support (XPS and RBS/ERD).

REFERENCES

(1) Waser, R.; Dittmann, R.; Staikov, G.; Szot, K. *Adv. Mater.* **2009**, *21*, 2632−2663.
(2) Tsuruoka, T.; Terabe, K.; Hasegawa, T.; Aono, M. *Nanotechnology* **2010**, *21*, 425205.
(3) Terabe, K.; Nakayama, T.; Hasegawa, T.; Aono, M. *Appl. Phys. Lett.* **2002**, *80*, 4009−4011.
(4) Sakamoto, T.; Sunamura, H.; Kawaura, H.; Hasegawa, T.; Nakayama, T.; Aono, M. *Appl. Phys. Lett.* **2003**, *82*, 3032−3034.
(5) Kozicki, M.; Park, M.; Mitkova, M. *IEEE Trans. Nanotechnol.* **2005**, *4*, 331−338.
(6) Kund, M.; Beitel, G.; Pinnow, C.-U.; Rohr, T.; Schumann, J.; Symanczyk, R.; Ufert, K.-D.; Muller, G. *Tech. Dig.−Int. Electron Devices Meet.* **2005**, 754−757.
(7) Kwak, J.; Chi, E.; Choi, J.; Park, S.; Baik, H.; So, M.; Lee, S. *J. Appl. Phys.* **1995**, *78*, 983−987.
(8) Wu, S.; Tsuruoka, T.; Terabe, K.; Hasegawa, T.; Hill, J. P.; Ariga, K.; Aono, M. *Adv. Funct. Mater.* **2011**, *21*, 93−99.
(9) Wang, Y.; Lv, H.; Wang, W.; Liu, Q.; Long, S.; Wang, Q.; Huo, Z.; Zhang, S.; Li, Y.; Zuo, Q.; Lian, W.; Yang, J.; Liu, M. *IEEE Electron Device Lett.* **2010**, *31*, 1470−1472.
(10) Liu, Q.; Long, S.; Wang, W.; Zuo, Q.; Zhang, S.; Chen, J.; Liu, M. *IEEE Electron Device Lett.* **2009**, *30*, 1335−1337.
(11) Schindler, C.; Weides, M.; Kozicki, M. N.; Waser, R. *Appl. Phys. Lett.* **2008**, *92*, 122910.
(12) Bernard, Y.; Renard, V. T.; Gonon, P.; Jousseaume, V. *Microelectron. Eng.* **2011**, *88*, 814−816.
(13) Goux, L.; Opsomer, K.; Degraeve, R.; Muller, R.; Detavernier, C.; Wouters, D. J.; Jurczak, M.; Altimime, L.; Kittl, J. A. *Appl. Phys. Lett.* **2011**, *99*, 053502.
(14) Kim, S.; Jo, M.; Park, J.; Lee, J.; Lee, W.; Hwang, H. *Electrochem. Solid-State Lett.* **2011**, *14*, 322−325.
(15) Aratani, K.; Ohba, K.; Mizuguchi, T.; Yasuda, S.; Shiimoto, T.; Tsushima, T.; Sone, T.; Endo, K.; Kouchiyama, A.; Sasaki, S.; Maesaka, A.; Yamada, N.; Narisawa, H. *Int. Electron Devices Meet.* **2007**, 783−786.
(16) Goux, L.; Opsomer, K.; Franquet, A.; Kar, G.; Jossart, N.; Richard, O.; Wouters, D.; Muller, R.; Detavernier, C.; Jurczak, M.; Kittl, J. *Thin Solid Films* **2013**, *533*, 29−33.
(17) *JCPDS Data Card no. 00−049−1411*; International Centre for Diffraction Data: Newtown Square, PA, 2004.
(18) Swain, B. P. *Surf. Coat. Technol.* **2006**, *201*, 1589−1593.
(19) Arezzo, F.; Zacchetti, N.; Zhu, W. *J. Appl. Phys.* **1994**, *75*, 5375−5381.
(20) Lee, W.-Y. *J. Appl. Phys.* **1980**, *51*, 3365−3372.
(21) King, M. O.; McLeod, I. M.; Hesp, D.; Dhanak, V. R.; Kadodwala, M.; MacLaren, D. A. *Surf. Sci.* **2012**, *606*, 1353−1359.
(22) Domashevskaya, E.; Gorbachev, V.; Terekhov, V.; Kashkarov, V.; Panfilova, E.; Shchukarev, A. *J. Electron Spectrosc. Relat. Phenom.* **2001**, *114*, 901−908.
(23) Neumann, H.; Mast, M.; Enderlein, J.; Tomlinson, R.; Yakushev, M. *Cryst. Res. Technol.* **1996**, *31*, 75−85.

(24) *JCPDS Data Card no. 01−089−4311*; International Centre for Diffraction Data: Newtown Square, PA, 2004.
(25) *JCPDS Data Card no. 01−085−0606*; International Centre for Diffraction Data: Newtown Square, PA, 2004.
(26) *JCPDS Data Card no. 00−045−1286*; International Centre for Diffraction Data: Newtown Square, PA, 2004.
(27) Pashinkin, A.; Fedorov, V. *Inorg. Mater.* **2003**, *39*, 539−554.
(28) *JCPDS Data Card no. 00−026−1117*; International Centre for Diffraction Data: Newtown Square, PA, 2004.
(29) *JCPDS Data Card no. 01−075−2078*; International Centre for Diffraction Data: Newtown Square, PA, 2004.
(30) Zhang, T.; Inoue, A.; Masumoto, T. *Mater. Trans., JIM* **1991**, *32*, 1005−1010.
(31) Wang, W.; Wei, Q.; Bai, H. *Appl. Phys. Lett.* **1997**, *71*, 58−60.
(32) Wang, W.; Bai, H. *J. Appl. Phys.* **1998**, *84*, 5961−5968.
(33) Goux, L.; Sankaran, K.; Kar, G.; Jossart, N.; Opsomer, K.; Degraeve, R.; Pourtois, G.; Rignanese, G.-M; Detavernier, C.; Clima, S.; Chen, Y.-Y; Fantini, A.; Govoreanu, B.; Wouters, D. J.; Jurczak, M.; Altimime, L.; Kittl, J. A. *IEEE Symp. VLSI Technol.* **2012**, 69−70.
(34) Yamano, Y.; Komiyama, T.; Takahashi, M.; Kobayashi, S.; Nitta, K.; Saito, Y. *23rd International Symposium on Discharges and Electrical Insulation in Vacuum*; IEEE: Piscataway, NJ, 2008; pp 35−38